



Spin singlet and quasiparticle excitations in cuprate superconductors

M. Mezidi ^{1,2}, A. Alekhin,¹ G. D. Gu,³ D. Colson,⁴ S. Houver,¹ M. Cazayous,¹ Y. Gallais,¹ and A. Sacuto ^{1,*}

¹Université Paris-cité, Laboratoire Matériaux et Phénomènes Quantiques, CNRS (UMR 7162), 75013 Paris, France

²Département de physique, Institut quantique and RQMP, Université de Sherbrooke, Sherbrooke, Québec, Canada.

³Matter Physics and Materials Science, Brookhaven National Laboratory (BNL), Upton, New York 11973, USA

⁴Université Paris-Saclay, CEA, CNRS, SPEC, 91191, Gif-sur-Yvette, France



(Received 19 July 2022; revised 25 October 2022; accepted 9 November 2022; published 23 November 2022)

We followed step by step the transition from an antiferromagnetic (AFM) Mott insulator to a superconducting (SC) metal in the $\text{Bi}_2\text{Sr}_2\text{CaCu}_2\text{O}_{8+\delta}$ (Bi-2212) cuprate using electronic Raman scattering spectroscopy. This was achieved by tracking the doping dependence of the spin singlet excitation (SSE) originating from the AFM Mott insulator, the normal-state quasiparticle excitation related to the mobile charge carriers, and the Bogoliubov quasiparticles related to the SC gap. We show that the signature of the pseudogap phase which develops during this transition can be interpreted as the blocking of charge carriers by the enhancement of the AFM correlations as the temperature drops. We find that the energy scale of the pseudogap, $\Delta_{\text{pg}}(p)$, closely follows that of the SSE, $\Delta_{\text{sse}}(p)$ with doping p . The quasiparticle lifetime considerably increases with doping when the pseudogap collapses. We reveal that the maximum amplitude of the SC gap $\Delta_{\text{sc}}^{\text{max}}$ and the SC transition temperature T_c are linked in an extended range of doping, such as $\Delta_{\text{sc}}^{\text{max}}(p) \propto \Delta_{\text{sse}}(p) T_c(p)$. This relation suggests that the AFM correlations play a key role in the mechanism of superconductivity.

DOI: [10.1103/PhysRevB.106.174513](https://doi.org/10.1103/PhysRevB.106.174513)

I. INTRODUCTION

The transformation from an antiferromagnetic (AFM) Mott insulator to a metal superconductor as the number of holes increases is a key element for understanding the physics of cuprates [1–8]. In the AFM Mott insulator phase, due to the strong onsite Coulomb repulsion U , electrons are localized on the copper sites, and their spins are AFM ordered along the Cu-O-Cu bonds in the copper oxygen planes due to the $J > 0$ exchange interaction constant. When a small fraction of electrons is removed from the copper oxygen plane, what is known as hole doping p , the AFM order is waning, and the electrons start to move. As the temperature decreases below T^* , an enigmatic phase emerges, the so-called pseudogap phase, which harbors several electronic orders [8–15]. At lower temperature, below T_c , the d -wave superconducting (SC) phase settles down. At higher doping level, the pseudogap phase disappears, giving way to a strange metal and then to a Fermi liquid metal, with which superconductivity persists and finally disappears when the hole doping increases. The AFM Mott insulator phase, the metallic phase, and the SC phase are respectively characterized by the spin singlet excitation (SSE) stemming from the AFM lattice, the quasiparticle excitation (QSPE) originating from the mobile charge carriers, and the Bogoliubov QSPE coming from the Cooper pairs breaking at twice the energy of the SC gap. All three excitations are detectable by electronic Raman spectroscopy.

In the past, most Raman studies were focused on the SSE (also called two-magnon) in cuprates. Its relationship with the

number of carriers or its interplay with the SC gap and its link to the pseudogap were investigated [16–24]. However, these studies were severely limited by the range of doping (above $p = 0.1$ and below $p = 0.20$), which led us to believe that, first, the energy scale of the pseudogap phase $\Delta_{\text{pg}}(p)$ and the maximum amplitude of the SC gap $\Delta_{\text{sc}}^{\text{max}}(p)$ are the same or very close to each other and, secondly, that the energy scale of the SSE $\Delta_{\text{sse}}(p)$ and $\Delta_{\text{sc}}^{\text{max}}(p)$ are proportional to each other as a function of doping.

Here, we show, by conducting an electronic Raman scattering study on Bi-2212 cuprate, over a larger range of doping from $p = 0.05$ to 0.23 and in an extended spectral range, that these two assertions are not valid over the full range of doping. We say that the $\Delta_{\text{pg}}(p)$ scale is distinct from $\Delta_{\text{sc}}^{\text{max}}(p)$, and it closely follows $\Delta_{\text{sse}}(p)$. By simultaneously tracking the doping dependence of the SSE and QSPE in the Raman spectra, we propose that the pseudogap opening as the temperature decreases is essentially due to the blocking of the charge carriers by the enhancement of the AFM correlations that originate from the parent AFM Mott insulator. This causes the loss of low-energy quasiparticle spectral weight when the temperature drops, as originally described in Refs. [25–28]. We find that the quasiparticle lifetime exponentially increases with doping when approaching the pseudogap end. Finally, we show that the energy of the SSE Δ_{sse} and the maximum amplitude of the SC gap $\Delta_{\text{sc}}^{\text{max}}$ are not proportional to each other but connected to T_c over a wide range of doping, such as $\Delta_{\text{sc}}^{\text{max}}(p) \propto \Delta_{\text{sse}}(p) T_c(p)$. We find this relation is consistent with earlier empirical laws extracted from other experimental techniques [29,30]. This relation suggests that the AFM correlations must be considered for understanding the cuprate SC state.

*alain.sacuto@u-paris.fr

II. RESULTS AND DISCUSSION

We performed electronic Raman measurements on the (Bi-2212) system over a large spectral range. This system has the advantage of allowing an exploration of its T - p phase diagram over a wide range of doping levels while only resorting to oxygen doping. Such a doping is much less invasive than cation insertion as done in YBCO or LSCO systems. The oxygen doped (Bi-2212) system has a maximum of $T_c = 90$ K. Details of the crystal growth and characterization are given in Refs. [31–33]. Electronic Raman scattering is a particularly useful probe for studying cuprate properties [34]. Indeed, it allows us to select distinct parts of the Brillouin zone, namely, the antinodal and nodal regions (see Appendix A for details). In the B_{1g} geometry, the Raman form factor is $(\cos k_x - \cos k_y)^2$, and it predominantly probes the antinodal region where the SC gap and the pseudogap are maximal, while in the B_{2g} geometry, the Raman form factor is $\sin^2 k_x \sin^2 k_y$, and it probes mostly the nodal region where the SC gap and the pseudogap are minimal. In this paper, we focus on the B_{1g} Raman response function from the $B_{1g} + A_{2g}$ response (cf. Appendix A). It turns out that the A_{2g} component is negligible in comparison with the B_{1g} one, as it will be shown in a future paper. The $\chi''_{B_{1g}+A_{2g}}(\omega, T = 104 \text{ K})$ Raman response of Bi-2212 single crystals from the underdoped (UD) to the overdoped (OD) regime is reported in Fig. 1(a). We see, at low doping (0.05–0.06), a well-defined and intense peak centered around 3000 cm^{-1} [indicated by a full arrow in Fig. 1(a)]. It is assigned to the SSE related to the AFM lattice. Its inelastic light scattering process is described in Figs. 2(a) and 2(b). The incoming photon is absorbed by moving an up spin to the neighboring site occupied by a down spin. The down spin then takes the place of the formerly up site, emitting an outgoing photon [36,37]. At the end of this process, six singlets are destroyed in the AFM lattice, and this costs an effective energy $2\Delta_{\text{sse}} = J_{\text{eff}} \approx 3J$. Here, J is the exchange interaction constant. As the doping increases, the AFM lattice breaks up, and the magnitude of the effective exchange interaction J_{eff} (initially equal to $3J$) decreases. The SSE mode is mainly detected in B_{1g} Raman response as predicted by the Loudon-Fluery model for a two-dimensional (2D), spin- $\frac{1}{2}$ Heisenberg system with only nearest neighbor interactions [36,38,39]. In the vicinity of the AFM insulator phase, the SSE peak location has been shown to give the first estimation of J in lanthanum and yttrium-based cuprates [16,17]. In (UD < 2 K) Bi-2212, we find $J \approx 125 \text{ meV}$ in good agreement with earlier works [20]. The SSE peak has a slightly asymmetrical profile in its high-energy side [Fig. 1(a)]. This was interpreted by extensions to the Loudon-Fluery model [37], including the triple resonant effect [36] and the magnon-magnon interactions mediated by the Higgs mode [40] recently supported by Raman study [23]. As the doping is increased, the SSE peak considerably broadens, and its maximum shifts to low energy from 3000 to 1500 cm^{-1} [Fig. 1(a)]. To thoroughly follow the evolution of the SSE peak from the very UD regime to the moderately UD regime, we have reported in Appendix B the Raman spectra of Bi-2212 in between $p \approx 0.06$ and 0.086 . We observe that the SSE peak softens in energy and broadens continuously as the doping increases. This is consistent with previous studies on other cuprates

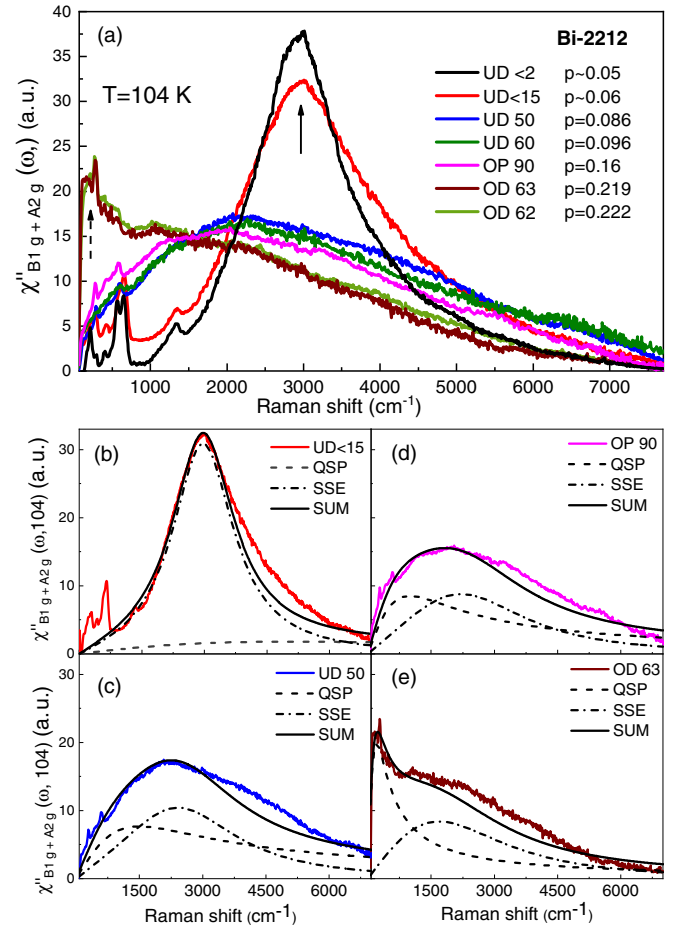


FIG. 1. (a) $\chi''_{B_{1g}+A_{2g}}(\omega)$ of Bi-2212 compound as a function of doping measured at $T = 104 \text{ K} > T_c$. The 532 nm excitation line was used. The initials UD, OP, and OD stand for underdoped, optimally doped, and overdoped. The numbers that follow the initials correspond to the T_c value. The doping level p was deduced from T_c using the Presland-Tallon law [35] and was corroborated by the energy of the pair-breaking peak (see Supplemental Material of Ref. [32]). (b)–(d) Fits of the Raman responses for several doping levels which highlight the spin singlet excitation (SSE) contribution (dashed-dotted line) and the quasiparticle excitation (QSPE; dashed line) are plotted.

[20–22]. Interestingly, when the doping reaches $p \approx 0.22$, a new peak emerges $< 500 \text{ cm}^{-1}$ [indicated by a dashed arrow in Fig. 1(a)]. We assigned this peak to the QSPE stemming from the mobile charge carriers. This peak is controlled by the scattering rate $\gamma \approx \frac{\hbar}{\tau}$, where τ is the quasiparticle lifetime. Its inelastic light scattering process is illustrated in Fig. 2(c). The energy is transferred from the photons to the charge carriers which gain kinetic energy [37,41]. In summary, as the doping increases, we observe that the high-energy SSE peak softens in energy and broadens and weakens in intensity, while the low energy QSPE peak grows up.

We propose a simple fit to highlight the balance effect between the SSE and the QSPE peak with doping. The slight asymmetry of the SSE peak line shape mentioned above will not be considered in this fit. We describe the SSE peak by the imaginary part of the linear response function of an harmonic

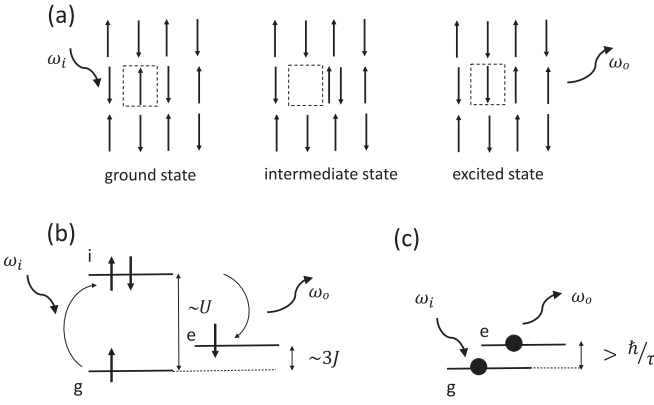


FIG. 2. (a) Spin singlet excitation (SSE) in the real space of an antiferromagnetic (AFM) lattice induced by inelastic light scattering. $\omega_{i,o}$ denotes, respectively, the energy of the incoming and outgoing photon. Energy diagram of the inelastic light scattering process for (b) a SSE in an insulator AFM lattice and (c) a quasiparticle excitation in a metal. The letters g, i, and e stand for the ground, intermediate, and final state.

oscillator with natural frequency $2\Delta_{\text{sse}}$ and damping γ_{sse} [42]:

$$\chi''_{\text{sse}}(\omega) = \frac{C_{\text{sse}}\omega}{\gamma_{\text{sse}}^2\omega^2 + [\omega^2 - (2\Delta_{\text{sse}})^2]^2}, \quad (1)$$

where $C_{\text{sse}} \propto \gamma_{\text{sse}}\Delta_{\text{sse}}$. The QSPE peak is described by the imaginary part of the electronic polarization [43] (often called the Drude response) and controlled by the damping γ_{qsp} :

$$\chi''_{\text{qsp}}(\omega) = \frac{C_{\text{qsp}}\omega}{\gamma_{\text{qsp}}^2 + \omega^2}, \quad (2)$$

where $C_{\text{qsp}} \propto \gamma_{\text{qsp}}\eta_{\text{F}}$. Here, η_{F} is the density of state at the Fermi energy. The Raman response $\chi''(\omega)$ is the sum of these two contributions. Selected fits are shown in Figs. 1(b)–1(e). They reproduce pretty well the experimental Raman spectra for several doping levels. We clearly see that the QSPE contribution (dashed line) forms gradually a hump ($\sim 1000 \text{ cm}^{-1}$) and then a narrow peak ($< 500 \text{ cm}^{-1}$) as the doping increases from the UD $> 15 \text{ K}$ to the OD 63 K Bi-2212 compound. This is consistent with the low-energy Raman response calculation based on the 2D Hubbard model [44]. Conversely, the SSE peak (dashed-dotted line) shifts to low energy and broadens and weakens in intensity. Our fits agree with the earlier computations [45] and the Raman response calculation from the 2D Hubbard model using cluster dynamical mean-field theory [46]. In this calculation, the total diagrammatic bubble part and the vertex correction correspond, respectively, to the QSPE and SSE contributions. We interpret the growing of the low-energy QSPE peak as the release of mobile charges when the AFM order is damaged by doping. The respective lifetimes of the SSE and QSPE extracted from the fits are reported in Fig. 3. They evolve in the opposite way with doping. At very low doping ($p \leq 0.06$), the lifetime of the SSE is larger than QSPE. Beyond $p = 0.15$, the QSP lifetime is larger than the SSE one. Interestingly, it exponentially increases when approaching $p = 0.22$. This specific doping was considered the ending point of the pseudogap phase in Bi-2212 cuprate [32,47], where changes in Fermi surface topology

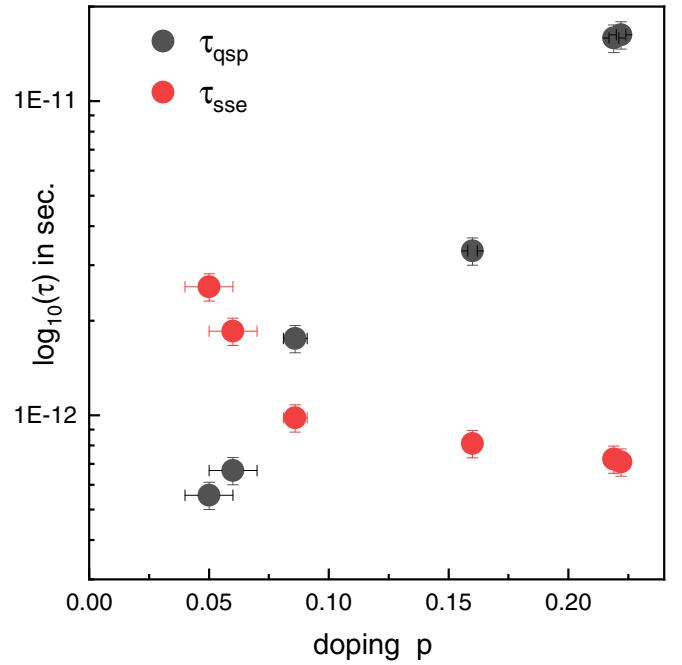


FIG. 3. Doping evolution of the spin singlet excitation and quasiparticle excitation lifetime. $\tau_{\text{sse/qsp}} = \frac{1}{c\gamma_{\text{sse/qsp}}}$, where c is the light velocity.

have been detected [32,48]. We now address the question of the pseudogap signature with temperature [7,25,26,28,49,50]. In Figs. 4(a)–4(c) are displayed the Raman responses of the UD $> 2 \text{ K}$, UD $< 15 \text{ K}$, and UD 50 K Bi-2212 compounds above and below T^* ($T = 295$ and 104 K , respectively). The pseudogap signature is highlighted by the blue shaded zone, which circumscribes the loss of low-energy spectral weight in the Raman response when the temperature is lowered from $T = 295$ to 104 K . We see that this loss decreases with doping. The low-energy Raman spectral weight at $p = 0.22$ (OD 62 K) exhibits a gain instead of a loss [indicated by a pink shaded zone in the inset of Fig. 4(d)]. The doping dependence of the subtracted Raman response $\Delta\chi''(\omega, 104\text{K}, 295\text{K}) = \chi''(\omega, 104\text{K}) - \chi''(\omega, 295\text{K})$ is plotted in Fig. 4(e). The crossing from spectral weight loss to weight gain is abrupt and indicated by an arrow near $p = 0.22$, where the pseudogap collapses. Let us focus on the strongly UD $< 2 \text{ K}$ Bi-2212 compound [Fig. 4(a)], where the pseudogap signature is strongest. We propose to interpret the pseudogap depletion by considering the balance effect between the QSPE and SSE as a function of temperature (instead of doping, as discussed above). Fits of the Raman responses measured at $T = 295$ and 104 K are reported in Figs. 4(f) and 4(g). These fits highlight the temperature dependence of the QSPE and SSE peaks. As the temperature decreases, the QSPE peak contribution (dashed line) is strongly reduced at low energy ($< 2000 \text{ cm}^{-1}$), while the SSE peak contribution (dash-dotted line) at higher energy becomes stronger and narrower $\sim 3000 \text{ cm}^{-1}$. The conjunction of these two phenomena produces the loss of low-energy spectral weight in the Raman response, as pointed out by the blue shaded zone in Fig. 4(a). The fit parameters are listed in Appendix C. The pseudogap is then interpreted by considering the enhancement of the AFM correlations

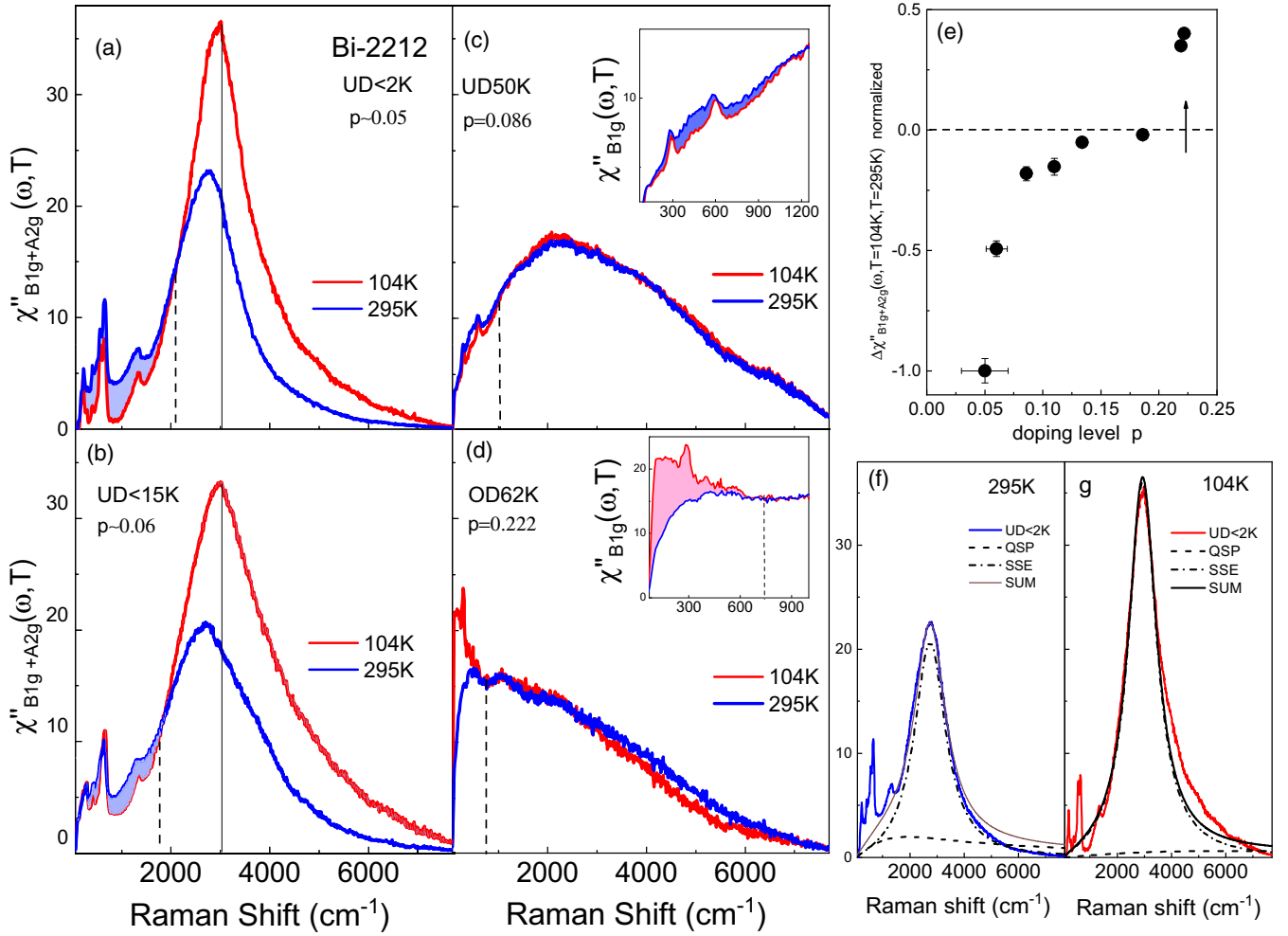


FIG. 4. (a)–(d) Raman response $\chi''_{B_{1g}}(\omega)$ of Bi-2212 at $T = 295$ and 104 K for selected doping levels. The blue shaded area underlines the pseudogap spectral weight depletion as the temperature is lowered below the dotted line. The inset of (c) shows a zoom of the pseudogap depletion. The hardening of the spin singlet excitation (SSE) peak as T decreases is underlined by the solid vertical line in (a) and (b). (e) Normalized doping dependence of $\Delta\chi''(\omega, 104\text{K}, 295\text{K}) = \chi''(\omega, 104\text{K}) - \chi''(\omega, 295\text{K})$. (f) and (g) Fits of the underdoped (UD) $< 2\text{K}$ Bi-2212 Raman responses at 295 and 104 K. The SSE and the quasiparticle excitation are, respectively, described by the dashed-dotted line and the dashed line.

upon cooling, which accentuates the blocking of the mobile charge carriers. The residual magnetic correlations are likely short range in space and dynamical in time and could be responsible for the pseudogap, as suggested theoretically before [46,51,52]. Our experimental observations and interpretation are compatible with the temperature dependence of the B_{1g} Raman response at low doping calculated for the 2D Hubbard model [46]. On the other hand, in the strongly OD regime, beyond the ending point of the pseudogap [OD 62 K Bi-2212, Fig. 4(d)], the low-energy QSPE becomes narrower and more intensive as the temperature decreases, giving rise to a well-defined low-energy peak, as expected for the metallic Raman response [37] and predicted by 2D Hubbard model computation [44,46].

So far, we have studied the balance effect between the low-energy QSPE and the high-energy SSE above T_c . Let us focus now on the relationship between the Bogoliubov QSPE and the SSE. In Fig. 5(a) are displayed the $B_{1g} + A_{2g}$ Raman responses of Bi-2212 single crystals over an extended range

of doping measured at low temperature ($T = 15$ K). At low doping ($p = 0.05$ and 0.06), the SSE is still at 3000cm^{-1} (indicated by arrows). The narrow features $< 1500\text{cm}^{-1}$ are phonon modes. The weak one at 1300cm^{-1} is a double phonon of the stronger one at 650cm^{-1} . These modes weaken with doping due to their scattering with the increased number of carriers. As the doping increases, we see that the SSE peak broadens to turn into a bump, and its maximum shifts to lower energy (2250cm^{-1} for $p \approx 0.1$) [cf. Fig. 5(b)]. For $p > 0.1$ [cf. Figs. 5(b) and 5(c)], the SSE hump softens in energy down to 1300cm^{-1} and fades away. The maximum of the hump disappears beyond $p = 0.22$ [see the dark blue curve of the OD 60 K Bi-2212 compound in Fig. 5(c)]. The weak feature observed $\sim 1300\text{cm}^{-1}$ is a double phonon already mentioned above. The superconductivity appears clearly in the $B_{1g} + A_{2g}$ spectra above $p \geq 0.10$. It manifests itself by a Cooper pair-breaking peak associated with the Bogoliubov QSPE [32,54–58]. It is labeled by a star in Figs. 5(b) and 5(c). In this geometry, the pair-breaking peak corresponds to the SC

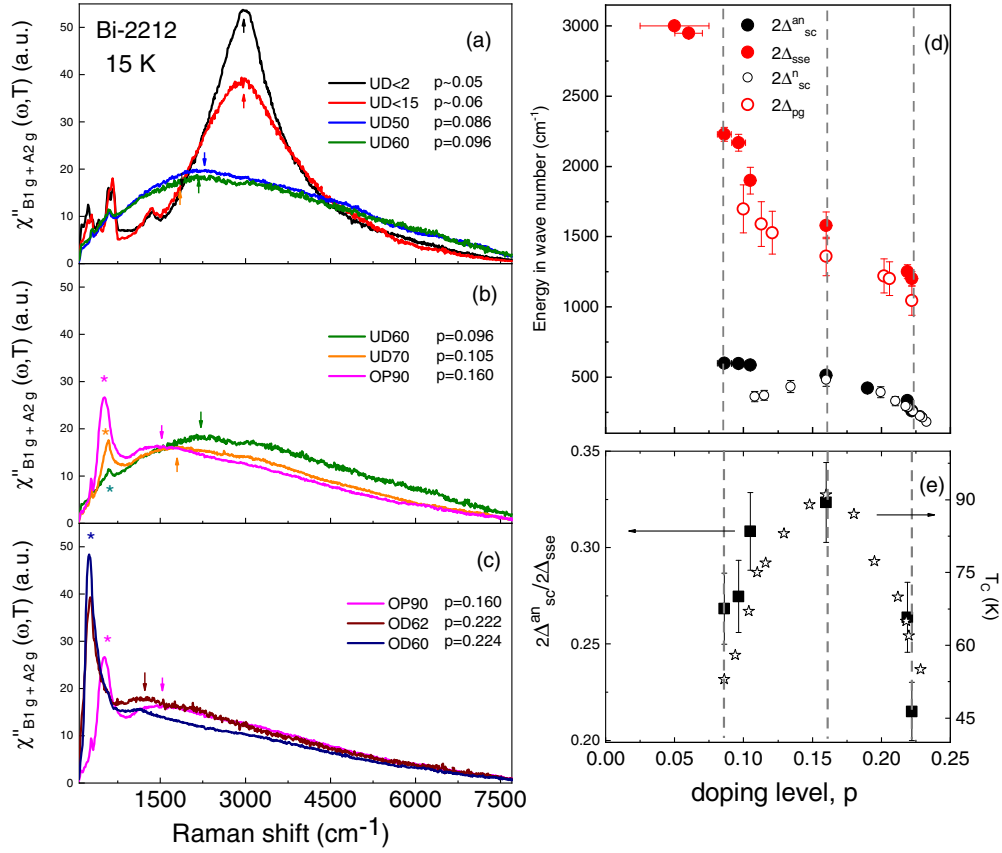


FIG. 5. (a)–(c) $\chi''_{B1g+A2g}(\omega, T)$ of Bi-2212 at $T = 15$ K for selected doping level. The arrows indicate the locations of spin singlet excitation (SSE) peaks and the stars the locations of the pair-breaking peaks. (d) Energy scale of the SSEs $2\Delta_{sse}$, the antinodal semiconducting (SC) gap $2\Delta_{sc}^{an}$ and the nodal SC gap $2\Delta_{sc}^n$ extracted from our previous works [53]. (e) Doping dependence of the $\frac{2\Delta_{sc}^{an}}{2\Delta_{sse}}$ ratio (black squares) which follows T_c (open stars). The dotted lines are guides for the eyes.

gap around its maximum amplitude, i.e., the antinodal SC gap. The pair breaking peak gets stronger with doping [Figs. 5(b) and 5(c)]. The SC pair-breaking peak is associated with a dip on its higher energy side, as it can be seen in the OP 90 Raman response [pink curve in Fig. 5(b)]. This originates from the interplay between the SC gap and the pseudogap in the antinodal region, as shown in our previous works [47,59,60]. The peak-dip-hump structure is also reproduced from other models [44,61].

The energy of the SSE $2\Delta_{sse}(p)$ (red filled circles) and the pseudogap $2\Delta_{pg}(p)$ (open red circle) are shown in Fig. 5(d). The $2\Delta_{pg}(p)$ plot was taken from Ref. [53]. Its energy was defined as the energy of the dip end (mentioned just above) and detected in the SC Raman response [53]. We see that both $2\Delta_{sse}(p)$ and $2\Delta_{pg}(p)$ decrease with doping, and they follow each other closely in the doping range where they were both measured. Moreover, they both disappear at the same doping level $p = 0.22$ where the pseudogap collapses [32,47]. This experimental observation leads us to conclude that $2\Delta_{pg}(p)$ and $2\Delta_{sse}$ correspond to the same energy scale.

The energy of the antinodal SC gap $2\Delta_{sc}^{an}$ (black filled circles) and that of the nodal SC gap $2\Delta_{sc}^n$ (open black circles) vs doping are displayed in Fig. 5(d). The energy of the nodal SC gap vs doping was taken from the Ref. [53]. The nodal SC gap is detected in the B_{2g} geometry and corresponds to the amplitude of the SC gap around the nodes. The energy of the

nodal SC gap follows a domelike shape approximately similar to that of the critical temperature T_c as a function of doping [described by open stars in Fig. 5(e)]. On the contrary the energy of the antinodal SC gap does not follow T_c and departs from the nodal SC gap in the UD regime. The distinct behavior between the nodal and antinodal SC gaps with doping has long been established by Raman scattering [34,37,58,62] and raised many questions (still debated), among which whether a relationship between the antinodal SC gap and T_c exists as is the case for the nodal SC gap.

In an attempt to clarify this last point, we focus first on the possible link between the energy of the SSE and the antinodal SC gap. We see in Fig. 5(d) that the energy of the SSE and the antinodal SC gap exhibit the same trend, i.e., decreasing with doping. However, they are not proportional to each other with doping, as suggested in earlier studies [19,22,24]. We find that the $\frac{2\Delta_{sc}^{an}}{2\Delta_{sse}}$ ratio vs doping [black square in Fig. 5(e)] is not a constant. It rather describes a domelike shape with a maximum close to the optimal doping $p = 0.16$ exactly like T_c , plotted as open stars in Fig. 5(e). This lead us to propose the following empirical relation:

$$2\Delta_{sc}^{an}(p) \propto 2\Delta_{sse}(p) T_c(p). \quad (3)$$

Since we have defined $2\Delta_{sse}(p) = J_{eff}(p)$, we get

$$2\Delta_{sc}^{an}(p) \propto \Delta_{sc}^{max}(p) \propto J_{eff}(p) T_c(p), \quad (4)$$

where $J_{\text{eff}}(p)$ links $2\Delta_{\text{sc}}^{\text{an}}(p)$ to T_c . This does not allow us to specify explicitly the role played by the AFM correlations in the SC pairing mechanism without theoretical calculations; even so, recent investigations carried out by other techniques support that Cooper pairing is driven by spin fluctuations in cuprates [63–66]. We hope that our empirical relation could be checked in the near future by cluster dynamical mean-field calculations of the Raman responses of the 2D Hubbard model in the SC state. This required computation of the Raman response over a large spectral range and large doping range so that the energies of $\Delta_{\text{sc}}^{\text{max}}(p)$ and $J_{\text{eff}}(p)$ could be estimated.

Finally, we would like to stress that this empirical relation is consistent with previous ones from different experimental techniques. As seen before, $J_{\text{eff}}(p)$ is related to the energy of the Raman SSE peak. It characterizes the strength of residual AFM correlations in the metallic phase state and their ability to block the mobile charge carriers as a function of doping p . On the other hand, the mobile charge carriers manifest themselves by the Raman QSPE peak whose intensity is related to the quasiparticle spectral weight at the antinodes $Z_{\text{an}}(p)$ [37]. As $J_{\text{eff}}(p)$ gets stronger, the number of charge carriers decreases, and therefore, $Z_{\text{an}}(p)$ decreases. It is then reasonable to conjecture that $J_{\text{eff}}(p) \propto \frac{1}{f[Z_{\text{an}}(p)]}$, where f is a monotonic function. The empirical relation in Eq. (4) becomes $\Delta_{\text{sc}}^{\text{max}}(p) f[Z_{\text{an}}(p)] \propto T_c(p)$. This relation is like the one proposed in Ref. [29] and based on angle-resolved photoemission spectroscopy measurements in UD Bi-2212 compounds. Indeed, they reported that the ratio $\frac{\Delta_{\text{sc}}^{\text{max}}(p) Z_{\text{an}}^{\text{arpes}}(p)}{T_c}$ is approximately a constant with doping. Here, $Z_{\text{an}}^{\text{arpes}}$ is the coherent quasiparticle spectral weight extracted from the spectral function at the antinodes.

More recently, the combination of Homes' law [30] in the dirty limit ($\sigma_{\text{dc}} \Delta_{\text{max}} \propto n_s$) and the Uemura law [67] valid in the UD regime ($n_s \propto T_c$) lead to $\sigma_{\text{dc}} \Delta_{\text{sc}}^{\text{max}} \propto T_c$, where n_s and σ_{dc} are, respectively, the superfluid density and the dc conductivity. This equation is also consistent with our empirical relation in Eq. (4), provided that $\sigma_{\text{dc}}(p) \propto \frac{1}{J_{\text{eff}}(p)}$. This is understandable if we consider that the stronger $J_{\text{eff}}(p)$ is, the more difficult it will be to move the carriers.

III. CONCLUSIONS

In conclusion, by simultaneously tracking the doping dependence of the SSE and QSPE respectively related to the AFM lattice and the mobile charge carriers, we can follow step by step the transition of the Bi-2212 cuprate from its Mott insulating AFM phase to its metallic phase. As the AFM order is damaged by doping, the mobile charge carriers are released and the QSPE lifetime exponentially increases when approaching the pseudogap end. We interpret the pseudogap effect with temperature as the blocking of mobile charge carriers by the enhancement of the AFM correlations as the temperature lowers. The pseudogap energy scale closely follows that of the SSE. In the SC state, we show that $2\Delta_{\text{sc}}^{\text{an}}(p) \propto J_{\text{eff}}(p) T_c(p)$. This empirical relation establishes an intriguing link between the antinodal SC gap and T_c and suggests that the effective exchange energy should play a key role in the SC mechanism.

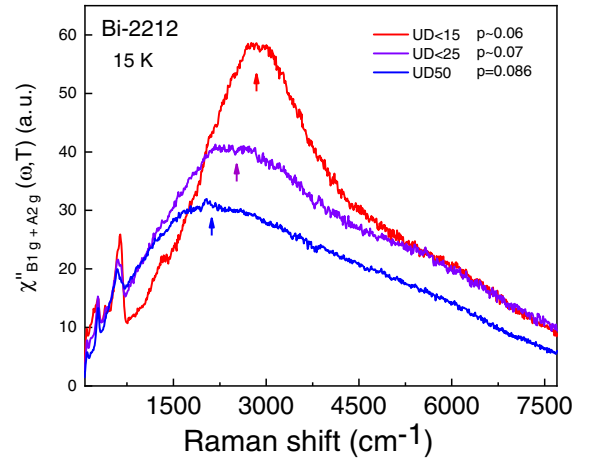


FIG. 6. (a) $\chi''_{B1g+A2g}(\omega)$ of Bi-2212 compound as a function of doping measured at $T = 15$ K. The 488 nm excitation line was used.

ACKNOWLEDGMENTS

We are grateful to L. Taillefer, A. Georges, A. Millis, I. Paul, M. Civelli, Y. Sidis, M. H. Julien and C. Proust for useful discussions. We acknowledge support from the French National Research Agency (ANR) Grant NEPTUN No. ANR-19-CE30-0019-01, the CNRS National Institute of Physics, and the Mission for Transversal and Interdisciplinary Initiatives (MITI) of the CNRS. Work at Brookhaven is supported by the Office of Basic Energy Sciences, Division of Materials Sciences and Engineering, U.S. Department of Energy under Contract No. DE-SC00112704.

APPENDIX A: DETAILS OF THE RAMAN EXPERIMENTS

Raman experiments were carried out using a JY-T64000 spectrometer in a single grating configuration using a 600 grooves/mm grating and Thorlabs notch filters to block the stray light. The spectrometer is equipped with a nitrogen-cooled back-illuminated 2048×512 charge-coupled device detector. We use the 532 and 488 nm excitation lines. Measurements between 10 and 295 K have been performed using an ARS closed-cycle He cryostat. This configuration allows us to cover a wide spectral range (70 to 8000 cm^{-1}) with a resolution set at 9 cm^{-1} . Each spectrum has been obtained from several frames centered on different wavelengths to cover the whole spectral range. Each frame is repeated twice to eliminate cosmic spikes, and acquisition time is ~ 10 mn. All spectra have been corrected for the Bose factor and the instrumental spectral response. They are thus proportional to the Raman response function $\chi''(\omega, T)$. The $B_{1g} + A_{2g}$ and $B_{2g} + A_{2g}$ Raman responses have been obtained from cross polarizations at 45° from the Cu–O bond directions and along them, respectively.

APPENDIX B: DOPING EVOLUTION OF THE SSE PEAK FROM STRONGLY TO MODERATE UD

We can clearly track the SSE peak position as a function of doping level. It shifts to low energy and it broadens as the doping increases (see the arrows in Fig. 6). The SSE peak intensity is ~ 1.5 higher than that measured with the

532 excitation line, and its high-energy asymmetric part is slightly enhanced. This is consistent with earlier Raman studies [16,18,23,68].

APPENDIX C: FIT PARAMETERS OF THE SSE AND QSPE PEAKS IN THE RAMAN RESPONSE

The fit parameters of the UD < 2 K Bi-2212 Raman responses are $\gamma_{sse} = 1400 \text{ cm}^{-1}$, $\gamma_{qsp} = 2000 \text{ cm}^{-1}$, and

$2\Delta_{sse} = 2800 \text{ cm}^{-1}$ for $T = 295 \text{ K}$; and $\gamma_{sse} = 1200 \text{ cm}^{-1}$, $\gamma_{qsp} = 6000 \text{ cm}^{-1}$, and $2\Delta_{sse} = 3000 \text{ cm}^{-1}$ for $T = 104 \text{ K}$. In these fits, we made the choice to increase the γ_{qsp} scattering rate rather than decrease the QSPE peak intensity; both options are possible. The fit parameters of the OD 62 K Bi-2212 Raman responses are $\gamma_{qsp} = 400 \text{ cm}^{-1}$, $\gamma_{sse} = 4800 \text{ cm}^{-1}$, and $\Delta_{sse} = 2600 \text{ cm}^{-1}$ for $T = 295 \text{ K}$; and $\gamma_{qsp} = 210 \text{ cm}^{-1}$, $\gamma_{sse} = 4600 \text{ cm}^{-1}$, and $\Delta_{sse} = 2500 \text{ cm}^{-1}$ for $T = 104 \text{ K}$.

-
- [1] P. W. Anderson, *Science* **235**, 1196 (1987).
 [2] D. Scalapino, *Phys. Rep.* **250**, 329 (1995).
 [3] J. Orenstein and A. J. Millis, *Science* **288**, 468 (2000).
 [4] M. R. Norman and C. Pépin, *Rep. Prog. Phys.* **66**, 1547 (2003).
 [5] A. Abanov, A. V. Chubukov, and J. Schmalian, *Adv. Phys.* **52**, 119 (2003).
 [6] P. A. Lee, N. Nagaosa, and X.-G. Wen, *Rev. Mod. Phys.* **78**, 17 (2006).
 [7] Y. Kohsaka, C. Taylor, P. Wahl, A. Schmidt, J. Lee, K. Fujita, J. W. Alldredge, K. McElroy, J. Lee, H. Eisaki *et al.*, *Nature* **454**, 1072 (2008).
 [8] B. Keimer, S. A. Kivelson, M. R. Norman, S. Uchida, and J. Zaanen, *Nature* **518**, 179 (2015).
 [9] B. Fauqué, Y. Sidis, V. Hinkov, S. Pailhès, C. T. Lin, X. Chaud, and P. Bourges, *Phys. Rev. Lett.* **96**, 197001 (2006).
 [10] T. Wu, H. Mayaffre, S. Krämer, M. Horvatić, C. Berthier, P. L. Kuhns, A. P. Reyes, R. Liang, W. N. Hardy, D. A. Bonn *et al.*, *Nat. Commun.* **4**, 2113 (2013).
 [11] R. Daou, J. Chang, D. LeBoeuf, O. Cyr-Choinière, F. Laliberté, N. Doiron-Leyraud, B. J. Ramshaw, R. Liang, D. A. Bonn, W. N. Hardy *et al.*, *Nature* **463**, 519 (2010).
 [12] G. Ghiringhelli, M. Le Tacon, M. Minola, S. Blanco-Canosa, C. Mazzoli, N. B. Brookes, G. M. De Luca, A. Frano, D. G. Hawthorn, F. He *et al.*, *Science* **337**, 821 (2012).
 [13] B. Loret, N. Auvray, Y. Gallais, M. Cazayous, A. Forget, D. Colson, M.-H. Julien, I. Paul, M. Civelli, and A. Sacuto, *Nat. Phys.* **15**, 771 (2019).
 [14] C. Proust and L. Taillefer, *Annu. Rev. Condens. Matter Phys.* **10**, 409 (2019).
 [15] M. Frachet, I. Vinograd, R. Zhou, S. Benhabib, S. Wu, H. Mayaffre, S. Krämer, S. K. Ramakrishna, A. Reyes, J. Debray *et al.*, *Nat. Phys.* **16**, 1064 (2020).
 [16] K. B. Lyons, P. A. Fleury, L. F. Schneemeyer, and J. V. Waszczak, *Phys. Rev. Lett.* **60**, 732 (1988).
 [17] K. B. Lyons, P. A. Fleury, J. P. Remeika, A. S. Cooper, and T. J. Negran, *Phys. Rev. B* **37**, 2353 (1988).
 [18] G. Blumberg, M. Kang, M. V. Klein, K. Kadowaki, and C. Kendziora, *Science* **278**, 1427 (1997).
 [19] S. Sugai and T. Hosokawa, *Phys. Rev. Lett.* **85**, 1112 (2000).
 [20] S. Sugai, H. Suzuki, Y. Takayanagi, T. Hosokawa, and N. Hayamizu, *Phys. Rev. B* **68**, 184504 (2003).
 [21] L. Tassini, W. Prestel, A. Erb, M. Lambacher, and R. Hackl, *Phys. Rev. B* **78**, 020511(R) (2008).
 [22] Y. Li, M. Le Tacon, M. Bakr, D. Terrade, D. Manske, R. Hackl, L. Ji, M. K. Chan, N. Barišić, X. Zhao *et al.*, *Phys. Rev. Lett.* **108**, 227003 (2012).
 [23] N. Chelwani, A. Baum, T. Böhm, M. Opel, F. Venturini, L. Tassini, A. Erb, H. Berger, L. Forró, and R. Hackl, *Phys. Rev. B* **97**, 024407 (2018).
 [24] L. Wang, G. He, Z. Yang, M. Garcia-Fernandez, A. Nag, K. Zhou, M. Minola, M. L. Tacon, B. Keimer, Y. Peng *et al.*, *Nat. Commun.* **13**, 3163 (2022).
 [25] H. Alloul, T. Ohno, and P. Mendels, *Phys. Rev. Lett.* **63**, 1700 (1989).
 [26] M. R. Norman, H. Ding, M. Randeria, J. C. Campuzano, T. Yokoya, T. Takeuchi, T. Takahashi, T. Mochiku, K. Kadowaki, P. Guptasarma *et al.*, *Nature* **392**, 157 (1998).
 [27] T. Timusk and B. Statt, *Rep. Prog. Phys.* **62**, 61 (1999).
 [28] J. Tallon and J. Loram, *Physica C* **349**, 53 (2001).
 [29] H. Ding, J. R. Engelbrecht, Z. Wang, J. C. Campuzano, S. C. Wang, H. B. Yang, R. Rogan, T. Takahashi, K. Kadowaki, and D. G. Hinks, *Phys. Rev. Lett.* **87**, 227001 (2001).
 [30] C. C. Homes, S. V. Dordevic, T. Valla, and M. Strongin, *Phys. Rev. B* **72**, 134517 (2005).
 [31] J. Wen, Z. Xu, G. Xu, M. Hücker, J. Tranquada, and G. Gu, *J. Cryst. Growth* **310**, 1401 (2008).
 [32] S. Benhabib, A. Sacuto, M. Civelli, I. Paul, M. Cazayous, Y. Gallais, M. A. Méasson, R. D. Zhong, J. Schneeloch, G. D. Gu *et al.*, *Phys. Rev. Lett.* **114**, 147001 (2015).
 [33] S. Benhabib, Y. Gallais, M. Cazayous, M.-A. Méasson, R. D. Zhong, J. Schneeloch, A. Forget, G. D. Gu, D. Colson, and A. Sacuto, *Phys. Rev. B* **92**, 134502 (2015).
 [34] M. Le Tacon, A. Sacuto, A. Georges, G. Kotliar, Y. Gallais, D. Colson, and A. Forget, *Nat. Phys.* **2**, 537 (2006).
 [35] M. R. Presland, J. L. Tallon, R. G. Buckley, R. S. Liu, and N. E. Flower, *Physica C* **176**, 95 (1991).
 [36] A. V. Chubukov and D. M. Frenkel, *Phys. Rev. B* **52**, 9760 (1995).
 [37] T. P. Devereaux and R. Hackl, *Rev. Mod. Phys.* **79**, 175 (2007).
 [38] P. A. Fleury and R. Loudon, *Phys. Rev.* **166**, 514 (1968).
 [39] J. B. Parkinson, *J. Phys. C* **2**, 2012 (1969).
 [40] S. A. Weidinger and W. Zwerger, *Eur. Phys. J. B* **88**, 237 (2015).
 [41] B. S. Shastry and B. I. Shraiman, *Phys. Rev. Lett.* **65**, 1068 (1990).
 [42] W. Hayes and R. Loudon, *Scattering of Light by Crystals* (Wiley, New York, 1978).
 [43] M. Klein, *Light Scattering in Solids I*, edited by M. Cardona (Springer-Verlag, Berlin, Heidelberg, 1982).
 [44] E. Gull and A. J. Millis, *Phys. Rev. B* **88**, 075127 (2013).
 [45] P. Prelovšek and J. Jaklič, *Phys. Rev. B* **53**, 15095 (1996).
 [46] N. Lin, E. Gull, and A. J. Millis, *Phys. Rev. Lett.* **109**, 106401 (2012).

- [47] B. Loret, S. Sakai, S. Benhabib, Y. Gallais, M. Cazayous, M. A. Méasson, R. D. Zhong, J. Schneeloch, G. D. Gu, A. Forget *et al.*, *Phys. Rev. B* **96**, 094525 (2017).
- [48] Y. Fang, G. Grissonnanche, A. Legros, S. Verret, F. Laliberté, C. Collignon, A. Ataei, M. Dion, J. Zhou, D. Graf *et al.*, *Nat. Phys.* **18**, 558 (2022).
- [49] K. Ishida, K. Yoshida, T. Mito, Y. Tokunaga, Y. Kitaoka, K. Asayama, Y. Nakayama, J. Shimoyama, and K. Kishio, *Phys. Rev. B* **58**, R5960 (1998).
- [50] F. Venturini, M. Opel, T. P. Devereaux, J. K. Freericks, I. Tüttő, B. Revaz, E. Walker, H. Berger, L. Forró, and R. Hackl, *Phys. Rev. Lett.* **89**, 107003 (2002).
- [51] B. Kyung, S. S. Kancharla, D. Sénéchal, A.-M. S. Tremblay, M. Civelli, and G. Kotliar, *Phys. Rev. B* **73**, 165114 (2006).
- [52] W. Wu, M. S. Scheurer, S. Chatterjee, S. Sachdev, A. Georges, and M. Ferrero, *Phys. Rev. X* **8**, 021048 (2018).
- [53] B. Loret, N. Auvray, G. D. Gu, A. Forget, D. Colson, M. Cazayous, Y. Gallais, I. Paul, M. Civelli, and A. Sacuto, *Phys. Rev. B* **101**, 214520 (2020).
- [54] F. Venturini, M. Opel, R. Hackl, H. Berger, L. Forró, and B. Revaz, *J. Phys. Chem. Solids* **63**, 2345 (2002).
- [55] K. C. Hewitt and J. C. Irwin, *Phys. Rev. B* **66**, 054516 (2002).
- [56] T. Masui, M. Limonov, H. Uchiyama, S. Lee, S. Tajima, and A. Yamanaka, *Phys. Rev. B* **68**, 060506(R) (2003).
- [57] S. Blanc, Y. Gallais, A. Sacuto, M. Cazayous, M. A. Méasson, G. D. Gu, J. S. Wen, and Z. J. Xu, *Phys. Rev. B* **80**, 140502(R) (2009).
- [58] N. Munnikes, B. Muschler, F. Venturini, L. Tassini, W. Prestel, S. Ono, Y. Ando, D. C. Peets, W. N. Hardy, R. Liang *et al.*, *Phys. Rev. B* **84**, 144523 (2011).
- [59] B. Loret, S. Sakai, Y. Gallais, M. Cazayous, M.-A. Méasson, A. Forget, D. Colson, M. Civelli, and A. Sacuto, *Phys. Rev. Lett.* **116**, 197001 (2016).
- [60] B. Loret, Y. Gallais, M. Cazayous, R. D. Zhong, J. Schneeloch, G. D. Gu, A. Fedorov, T. K. Kim, S. V. Borisenko, and A. Sacuto, *Phys. Rev. B* **97**, 174521 (2018).
- [61] A. V. Chubukov, D. K. Morr, and G. Blumberg, *Solid State Commun.* **112**, 183 (1999).
- [62] W. Guyard, M. Le Tacon, M. Cazayous, A. Sacuto, A. Georges, D. Colson, and A. Forget, *Phys. Rev. B* **77**, 024524 (2008).
- [63] M. Le Tacon, G. Ghiringhelli, J. Chaloupka, M. M. Sala, V. Hinkov, M. W. Haverkort, M. Minola, M. Bakr, K. J. Zhou, S. Blanco-Canosa *et al.*, *Nat. Phys.* **7**, 725 (2011).
- [64] F. Restrepo, U. Chatterjee, G. Gu, H. Xu, D. K. Morr, and J. C. Campuzano, *Commun. Phys.* **5**, 45 (2022).
- [65] S. O'Mahony, W. Ren, W. Chen, Y. X. Chong, X. Liu, H. Eisaki, S. Uchida, M. Hamidian, and J. S. Davis, *PNAS* **119**, e2207449119 (2022).
- [66] Q. Ma, E. M. Smith, Z. W. Cronkwright, M. Dragomir, G. Mitchell, A. I. Kolesnikov, M. B. Stone, and B. D. Gaulin, *Phys. Rev. Res.* **4**, 013175 (2022).
- [67] Y. J. Uemura, G. M. Luke, B. J. Sternlieb, J. H. Brewer, J. F. Carolan, W. N. Hardy, R. Kadono, J. R. Kempton, R. F. Kiefl, S. R. Kreitzman *et al.*, *Phys. Rev. Lett.* **62**, 2317 (1989).
- [68] S. Sugai, S.-i. Shamoto, and M. Sato, *Phys. Rev. B* **38**, 6436 (1988).